Tectonophysics 498 (2011) 35–44

Contents lists available at ScienceDirect

Tectonophysics

journal homepage: www.elsevier.com/locate/tecto

A coupled fluid-fracture approach to propagation of clastic dikes during earthquakes

Tsafrir Levi [a,*], Ram Weinberger [a], Yehuda Eyal [b]

[a] Geological Survey of Israel, 30 Malkhe Israel 95501, Jerusalem, Israel
[b] Department of Geological and Environmental Sciences, Ben Gurion University of the Negev, Beer Sheva, Israel

ARTICLE INFO

Article history:
Received 16 September 2009
Received in revised form 20 June 2010
Accepted 23 November 2010
Available online 30 November 2010

Keywords:
Clastic dikes
Propagation
Hydro-fracturing
Dead Sea fault
Seismites

ABSTRACT

The propagation of clastic dikes was studied in Ami'az Plain, where hundreds of clastic dikes cross-cut the soft rock of the late Pleistocene lacustrine Lisan Formation, within the seismically active Dead Sea basin. Two analytic models were established to estimate the dike propagation velocities, the dike emplacement duration, and the driving pressures that were associated with dike propagation either under laminar or turbulent flow conditions. These models depend on the host-rock and fluid properties, dike width and length. Based on these properties and field limitations, the results indicate that the dikes were propagated under turbulent flow conditions and propagation velocities of ~4–65 m/s. The emplacement duration of the clastic dikes is between ~0.8 and 2 s, which is similar to the order of the acoustic wave duration that passes through the soft rock during an earthquake event. This implies that the propagation of dikes could form during the passing acoustic waves and may thus be considered as an earthquake-induced impact structures. The calculated driving pressures that were generated during the earthquake events near the surface are 1–2 MPa, one order of magnitude larger than the pressure due to the overburden on the source layer.

1. Introduction

Earthquake-induced clastic dikes are formed by injection of clastic material into the host rock and associated with overpressure buildup and dynamic fracturing (e.g., Obermeier, 1996, 1998; Levi et al., 2009). Estimations of the duration and the driving pressures associated with the clastic dike propagation induced by earthquakes provide further insight on the physical conditions magnitude and location of paleo-earthquakes. Earthquake-induced clastic dikes are natural example of hydraulic fractures (e.g., Pollard, 1987; Pollard and Segal, 1987; Lister, 1990; Rubin, 1995; Vigorito et al., 2008). As such, their propagation couples two processes; fracture propagation (e.g., Anderson, 1995) and flow of clastics. The flow itself is a complex process because it may involve laminar or turbulent conditions. The rate of the fracture propagation and growth (in term of length, height and width) mainly depends on the fluid viscosity, the host-rock strength and the driving pressures (Rodrigues et al., 2009). The propagation rate and emplacement duration of clastic dikes are not well constrain, and seldom studied in depth. Although the estimated propagation rate of the injection clastic dikes is important, so far no study has been done on the injection clastic dikes propagation. Until this study, only a few works estimated the emplacement duration of the clastic dikes based on steady-state flow rate in conduits and channels (Gallo and Woods, 2004; Levi et al., 2008). Yet, previous estimations were not based on a coupled fluid-fracture approach.

Natural structures associated with hydro-fracturing such as joints (e.g., Eyal et al., 2001; Weinberger and Bahat, 2008), veins, magmatic dikes (e.g., Weinberger et al., 1995) and injection clastic dikes (e.g., Hurst and Cartwright, 2007; Vigorito and Hurst, 2010) represent propagation under different rates. Joint or vein propagation may extend for a long period (i.e., years) due to continuous tectonic loading (e.g., Bahat, 1991 and references therein). Magmatic dikes typically propagate over short periods of hours or days, depending on the magma viscosity, depth of emplacement and host-rock properties (Rubin, 1993). In magma flow conditions, when the fluid viscosity is between 10^2 and 10^5 Pa s, a laminar flow condition is more adequate (Turcotte and Schubert, 1982), and slow propagation (~0.1 m/s) is expected. Low viscosity (10^{-1} Pa s) characterizes the fluidized sediments during the propagation of clastic dikes leading to turbulent flow conditions and fast propagation (>1 m/s) (Turcotte and Schubert, 1982).

Hundreds of clastic dikes are exposed in the seismically active Dead Sea basin (Ami'az Plain study area, Fig. 1). Previous studies (Levi et al., 2006a,b) demonstrated that the clastic fill of these dikes is connected to a clay-rich source layer, and were formed by injection of this fluidized layer into the fractures during strong (M>6.5) Holocene earthquake events. Such intrusions could occur only if the source layer was under high-pressure relative to the surrounding host rock, and that pressure difference between the fluidized clastic material in the source layer and the propagating fracture (dike) was sustained during the intrusion. This pressure difference leads to dilation of the fracture and enables the clastic material to flow through the fracture. Once the excess pressure in

* Corresponding author. Tel.: +972 02 5314263.
E-mail address: tsafrir@gsi.gov.il (T. Levi).

0040-1951/$ – see front matter © 2010 Elsevier B.V. All rights reserved.
doi:10.1016/j.tecto.2010.11.012

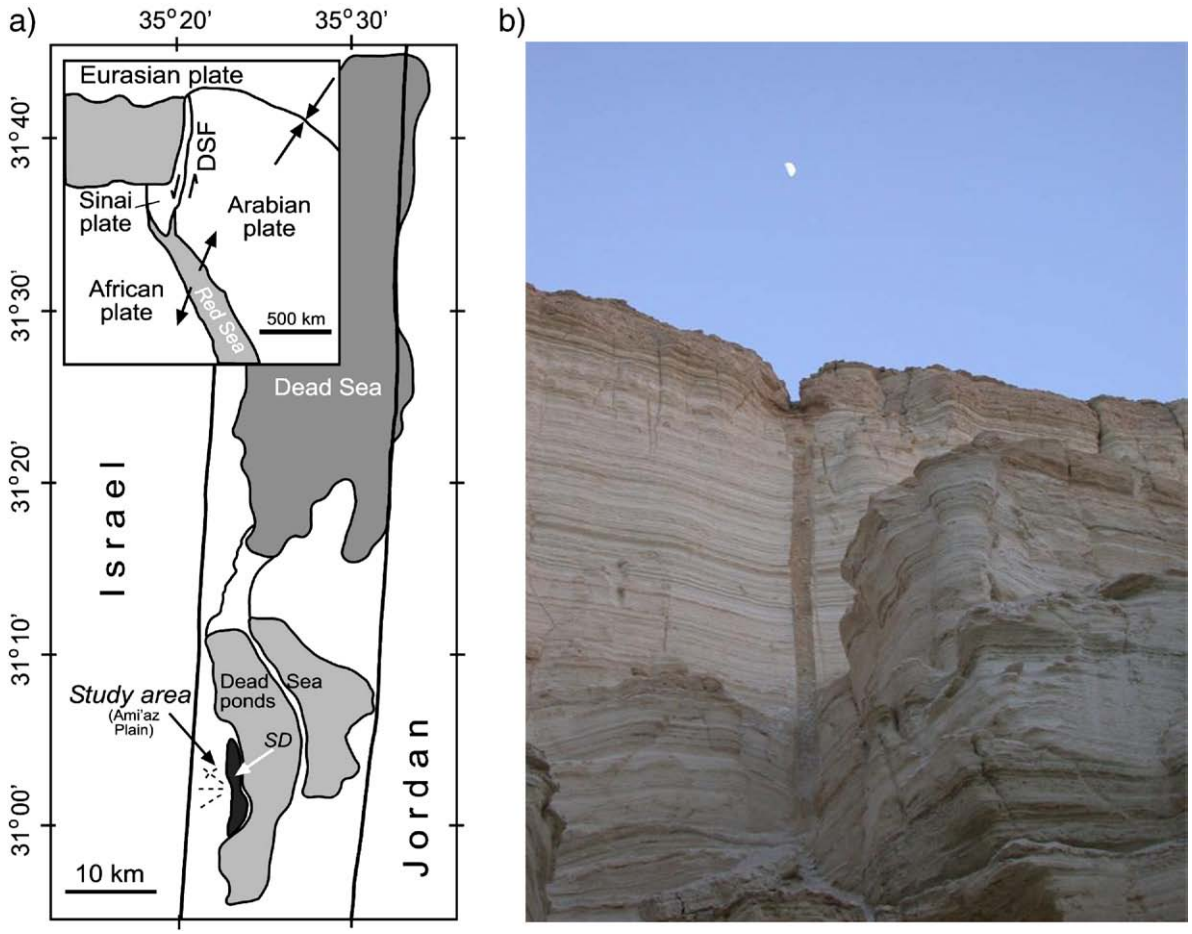

Fig. 1. Location maps of the study area. a: The Dead Sea Fault and Ami'az Plain with the clastic dikes marked schematically by dashed lines. DSF, Dead Sea Fault; SD, Sedom Diapir (Zak, 1967; Weinberger et al., 2006); inset: the regional setting of the tectonics plates adjacent to the Dead Sea Fault. b: photograph of a clastic dike in the study area.

the clastic dike decreases fracture propagation ceases and the injection process terminates.

There are several strong arguments for the origin of the clastic dikes in Ami'az Plain like as follows: (1) A physical connection exists between the clastic infill material and the source clay-rich layers, indicating upward transport of clastic material, (2) a similar mineral assemblage in both the source layers and the clastic material in the dikes, and (3) the AMS (anisotropy of magnetic susceptibility) analysis of the dike's infill shows a injection fabric compatible with upward and lateral components of flow directions (see below). Furthermore, Levi et al. (2006a,b) suggested that the formation of the injection dikes were induced by earthquakes along one of the faults comprising the active Dead Sea fault system. These events occurred, based on a resetting of quartz Optically Stimulated Luminescence (OSL) signals, between 15,000 and 7000 years B.P. (Porat et al., 2007).

Levi et al. (2006b) analyzed the magnetic fabric of the clastic dikes and demonstrated that the AMS signals resulted from fast flow conditions. The AMS analysis revealed that the propagation of the dikes was mainly upward but, in many cases the propagation was laterally due to stiff gypsum layers that form mechanical boundaries below the source layer and above it near the surface. The AMS analysis also revealed that although the flow direction was mainly upward, small eddies were generated along the dike walls. This implies that at the final stage of dike emplacement the particle–water mixture filled the entire dike width and the flow was fully turbulent.

Yet, the flow conditions (laminar/turbulent) during clastic-dike propagation are not known and different propagation rate and pressure gradients may result due to varied flow conditions. Laminar or turbulent flow conditions may exist during different stages of clastic dike emplacement. Hence, the aim of this study is to quantify the dike propagation rate based on analytical equations of propagation and geological constrains, and estimate the emplacement duration of the clastic dikes and the associated driving pressures. The study combines for the first time with three important matters, including fracture propagation, clastic flow conditions, and accurate clastic-dike dimensions that help to constrain the model results. We adopted two mechanical models for either laminar or turbulent flows during clastic dikes propagation which initially were developed for propagation of magmatic dikes (Turcotte et al., 1987). The duration of the clastic dikes and the driving pressures obtained in this study shed light on the clastic-dike propagation during earthquake events.

2. Geologic setting

The Dead Sea basin is a continental depression, which is bounded on the east and west by a series of oblique-normal faults. The Ami'az Plain study area (Fig. 1), located near the southwestern margin of the Dead Sea basin, within the Dead Sea fault system (e.g., Quennell, 1959a,b; Freund, et al., 1968; Garfunkel, 1981) is one of the western downfaulted blocks of this depression.

The incision of Nahal (Wadi) Perazim in Ami'az Plain exposes the entire section (~40 m thick) of the Lisan Formation, and about 250 are relatively large-scale (height, length >10 m) clastic dikes, which cut through the section. The age of the Lisan Formation, based on U–Th dating, ranges between ~70,000 and 15,000 years B.P. (Haase-Schramm et al., 2004). The Lisan Formation consists mostly of authigenic (chalk) aragonite laminae alternating with fine detritus layers (Begin et al., 1980). The upper part of the Lisan Formation consists of a ~1 m thick,

relatively stiff gypsum layer. A thin veneer (<1 m) of eolian and fluvial sediments overlies the formation, and covers large parts of the plain. A few thick green, clay-rich layers are exposed at the lower part of this formation. Shaking such clay-rich layers causes a drastic loss of shear strength, and a consequent pressure buildup and particle-water flow (Arkin and Michaelli, 1986).

The injection clastic dikes are composed of green clay, silty quartz, and some aragonite fragments. The dike heights vary between 5 mm and 18 m, and the dike widths between 1 mm and 0.18 m. However, the width of the large dikes (>10 m) is generally greater than 7 mm. Measuring the lengths of the large-scale dikes on air-photos indicates that they vary between 20 and 70 m, and the average is about 55 m (Fig. 2). Most of the clastic dikes in Ami'az Plain are injected structures and only a few were formed by passive deposition of clastic material within pre-existing tensile fissures (Levi et al., 2006a,b). The paleoseismic record from the Dead Sea basin based on breccia layers reveals numerous moderate to strong earthquake events during the late Pleistocene (e.g., Marco and Agnon, 1995; Begin et al., 2005), and during the Holocene (Enzel et al., 2000; Ken-Tor et al., 2001; Begin et al., 2005). The strongest recorded event in the Dead Sea basin is the M = 6.2 earthquake of July 11, 1927, whose focal mechanism solution, was a left-lateral motion (Ben-Menahem et al., 1976; Shapira et al., 1993). The strongest instrumentally recorded event along the Dead Sea fault is the $M_w = 7.2$ November 22, 1995 Gulf of Aqaba earthquake (Hofstetter, 2003).

3. Mechanical modeling of the dike propagation

3.1. Assumptions and justifications

The model assumptions for the dike propagation and their justifications are based on field observations (Levi et al., 2008, 2009), AMS analysis (Levi et al., 2006a,b), and OSL dating (Porat et al., 2007). The emplacement of the dikes may be divided into three consequent stages: (1) pressure buildup triggered by the impact of the seismic wave within the source layer up to a fracture nucleation in the overlying Lisan strata and fluidization of the clay-rich layers; (2) propagation of pressure-driven fractures which is followed by injection of clastic material that consequently fills the fractures (Fig. 3a); and (3) pressure decrease and fracture arrest. Hence we assume that a mean steady-state flow is achieved during the clastic dike propagation (i.e., stage 2); this assumption is related to both laminar and turbulent flow conditions.

3.2. Analytic approaches for dike propagation

The clastic dikes are blade-like dikes (y<x<z; Fig. 3) and propagate upward and laterally. The x, y, z coordinates parallel the dike height, width and, length respectively, and are centered in the middle of the dike (Fig. 3). The present study checks the horizontal component of propagation, parallel to the z direction, that resulted from the driving pressure (Δp) existing within the dike, and by the stress concentration at the dike peripheries.

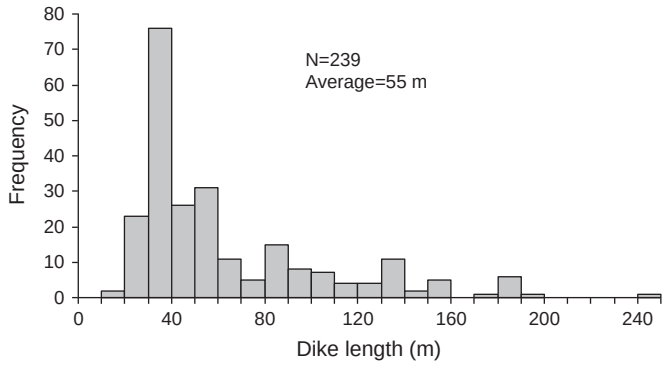

Fig. 2. A diagram showing the frequency of clastic-dike lengths. Measurements of dike lengths are based in Fig. 1 in Marco et al. (2002).

The dike shapes are controlled by the elastic deformation of the host rock, and their measured dimensions are used for constraining the dike propagation models. The present model starts from a penny-shaped dike (y<x = z), which is bordered by the upper and the lower gypsum layers. Further, the model continues describing a blade-like dike, which propagates parallel to the z axis (Fig. 3). The range of dike widths ($2w$) is between 0.07 and 0.2 m and the range of the dike lengths ($2\,l$) is between 18 m for the disk-shaped dike and ~75 m for the blade-like dike.

Clastic dike propagation is a coupled fluid and elastic-fracturing processes in which the flow rate for the fluid within the fracture must be solved simultaneously with the elastic deformation of the host rock. In the present study, the near surface propagation of the clastic dike is mainly controlled by the injection pressure. Laminar and turbulent flow conditions depend on different pressure gradient (dp/dz). Therefore, it is important to know the flow condition and the associated dike propagation velocities and driving pressures (Δp).

For analyzing the dynamics of the clastic dikes development we adopted the analytical model of Turcotte et al. (1987) for dike propagation. This model is based on the stress intensity (Ki) criterion for propagation, and on solving equations for a fluid-driven fracture. It illustrates the basic mechanisms of clastic dike propagation under laminar and turbulent flow conditions. Other analytic approaches that were developed to describe fracture/dike propagation were based on the cohesive zone model, which is associated with the dike edges (Barenblatt, 1962; Rubin, 1993, 1995). We do not use these models because Levi et al. (2009) showed that the relations between the cohesive (tip)-zone height and dike height are non-linear, suggesting that the cohesive (tip)-zone model for the clastic dike propagation in Ami'az Plain is questionable.

In the present model the fracture width along the dike center, $2w(0)$, the half fracture length, l, and the driving pressure in the dike center, $\Delta p(0)$ depend on the dike emplacement duration t (Fig. 2). The model assumes that the injected clastic material (particle–water mixture) behaves as Newtonian fluid (see sets of laboratory experiments which justify this assumption in Levi et al., 2008). During propagation the flow rate is $A = Re\ \eta/\rho_f$ (Prandtl, 1942), in which Re the Reynolds number, η the dynamic viscosity, and ρ_f the fluid density, are constant. The Reynolds number controls the transition from laminar to turbulent flow. The onset of turbulent flow in the dike occurs at $Re \approx 2.2 \times 10^3$ (e.g., Turcotte and Schubert, 1982; Donald, 1995). Substituting $Re \approx 2.2 \times 10^3$ into the flow rate equation enables the estimation of a high flow rate for the laminar condition and a low flow rate for turbulent condition.

The dike widths were measured accurately in the field; hence the range of the dike emplacement duration t is set by substituting the dike width interval. Because the dike grew simultaneously in all directions, the range of the t increments should be the same as those of the dike width $2w$ (0.07–0.2 m) and the half-dike length l (~10–40 m; see the section Geologic setting).

Under laminar flow conditions the dike emplacement duration is (Turcotte et al., 1987)

$$t = \frac{2w(0)^3}{C_2{}^3 A^{3/2} \left(\frac{\eta(1-\upsilon)}{G}\right)^{1/2}}, \tag{1}$$

and the half dike length l is:

$$l = C_1 A^{1/2} \left[\frac{G}{(1-\upsilon)\eta}\right]^{1/6} t^{2/3}, \tag{2}$$

in which υ is the Poisson's ratio, G is the shear modulus, A is the flow rate and $C_1 = 0.589$ $C_2 = 1.698$ are the equation constants.

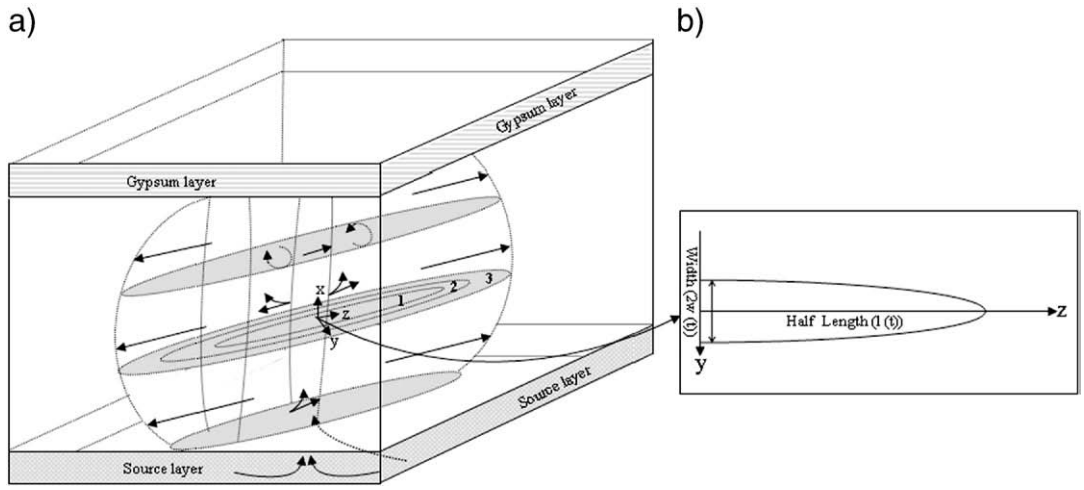

Fig. 3. Schematic representation of the geometry and propagation of a clastic-dike. (a) Blade-like dike parallel to the horizontal z-axis. The clastic material is mainly transported horizontally between the source layer and the upper gypsum layer as well as upwards. The dike length, width and height are time dependent, and the marked numbers represent their growth stages. Lateral propagation along the z-axis and dilation parallel to y-axis. (b) The coordinate system is located at the center of the dike.

By setting the range of dike width (0.07–0.2 m), the range of dynamic viscosity (0.05–0.3 Pa s) (Levi et al., 2008) and $Re \leq 2.2\times10^3$, a range of t can be calculated. The half-dike lengths are set by substituting the emplacement duration t using Eq. (1). The driving pressure $\Delta p(0)$ that acts on the dike walls is calculated by substituting the dike emplacement duration t, as follows (Turcotte et al., 1987):

$$\Delta p(0) = C_3 A^{1/2}\left(\frac{G}{1-\upsilon}\right)^{2/3}\left(\frac{\eta}{t}\right)^{1/3}, \tag{3}$$

in which $C_3 = 1.44$ is the laminar equation constant.

Based on the flow rate, and the calculated emplacement duration, the propagation velocity for half dike length l (dl/dt) can be calculated.

Under turbulent flow conditions the emplacement duration is

$$t = \frac{2w(0)^3 G^{1/2}}{C_5{}^3 A^{15/8}\rho^{3/8}\eta^{1/8}(1-\upsilon)^{1/2}}, \tag{4}$$

and the half-dike length is:

$$l = C_4\frac{A^{3/8}G^{1/6}t^{2/3}}{\rho_{fluid}{}^{1/8}\eta^{1/24}(1-\upsilon)^{1/6}}, \tag{5}$$

in which $C_4 = 1.40$ and $C_5 = 0.714$ are the turbulent equation constants. The dike emplacement durations are calculated by the same procedure as mentioned above for laminar flow. However, $Re \approx 2.2\times10^3$ in the turbulent condition gives the upper limit of the emplacement duration values.

The driving pressure $\Delta p(0)$ that acts on the dike walls is calculated by substituting the emplacement duration t, as follows (Turcotte et al., 1987):

$$\Delta p(0) = C_6\frac{A^{1/4}\rho_{fluid}{}^{1/4}\eta^{1/12}G^{2/3}}{(1-\upsilon)^{2/3}t^{1/3}}, \tag{6}$$

in which $C_6 = 0.255$ is the turbulent equation constant. Based on the flow rate, and the calculated t, the propagation velocity dl/dt for the turbulent flow conditions can be calculated.

The magnitude of the static pressure, within the center of the blade-like dike is at least the sum of the fluid weight (~0.1 MPa) and the atmospheric pressure (0.1 MPa), and hence, cannot be lower than ~0.2 MPa.

During the dike propagation, the leading fracture edges might be associated with dynamic fracturing. Levi et al. (2008), estimated the dynamic fracturing velocity by using the equation $u_{upper} \leq u_{dynamic} \leq 0.5(G/\rho_r)^{0.5}$, where ρ_r is the rock density. Theoretically, the dike propagation velocity cannot be higher than the dynamic fracturing velocity (Freund, 1998). Thus, the dynamic fracturing velocity is used here as the upper velocity limit for clastic-dike propagation.

4. Results

4.1. Laminar flow model conditions

For estimating the mechanical properties of the Lisan sediments we used published data on comparable soft sediments (see Table 1). The laminar models start by calculating the emplacement duration for certain dike widths (Eq. (1)) using different flow rates.

The runs were performed by setting the Re range between 1×10^2 and 2.2×10^3, and two dynamic viscosities (0.05 and 0.3 Pa s). The calculated dike emplacement duration for the laminar flow conditions varies between 9 and ~600×10^3 s (Fig. 4). The shortest emplacement duration was obtained for a dike width of 0.07 m, dynamic viscosity of 0.3 Pa s, and $Re = 2.2\times10^3$ (Fig. 4, run d). The longer emplacement duration was obtained for a dike width of 0.2 m, dynamic viscosity of 0.05 Pa s, and $Re = 1\times10^2$ (Fig. 4, run a).

Table 1
Variables of soft sediments and clastic dikes used for calculations.

Variable	Symbol	Values	Source
Dike width	$2w$	0.07–0.2 m	Field observations
Dike length (average)	$2l$	55 m	Field observations (Fig. 2)
Poisson's ratio	υ	0.4	Gee-Clough et al., 1994; Vallejo1 and Lobo-Guerrero, 2002; Chetrit, 2004; Othman, 2005; Bala et al., 2006
Dynamic viscosity	η	0.05–0.3 Pa s	Levi et al., 2008
Fluid density	ρ_f	1700–1950 kg/m^3	Levi et al., 2008
Rock density	ρ_r	1400 kg/m^3	Levi et al., 2008
Shear modulus	G	100 MPa	Gannon et al., 1999; Schneider et al., 1999; Yuan-qiang and Xu, 2004; Chetrit, 2004; Bala et al., 2006
Tensile strength	T	0.1 MPa	Arkin and Michaeli 1986
Yielding stress	σ_{YS}	0.4 MPa	Karig, 1996
Grain diameter	d	5×10^{-5} m<	Present study
Density of the fluidized grains	ρ_s	2650 kg/m^3	Bell, 2000

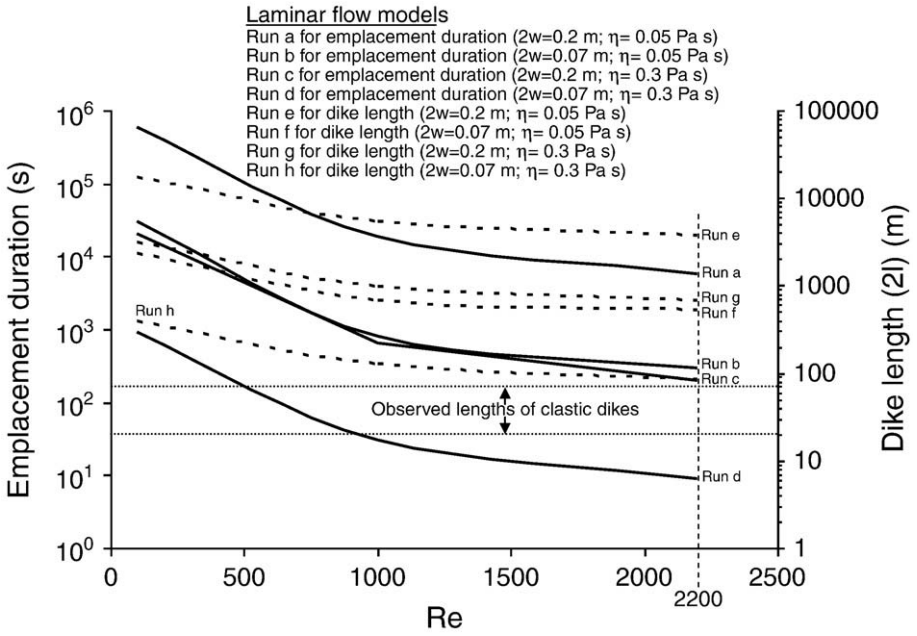

Fig. 4. Results of the laminar propagation model, showing the emplacement duration and dike length as a function of *Re* number plotted on a log–log–linear graph (Eqs. (1) and (2)). Solid lines mark the emplacement duration in seconds, and the dashed lines mark the clastic-dike lengths. A range of observed lengths of clastic dikes is marked by two dashed lines.

The range of the emplacement durations calculated by Eq. (1) was used for calculating the ranges of dike length (Eq. (2)), driving pressure (Eq. (3)) and dike propagation velocity d*l*/d*t* (Fig. 7). The calculated dike lengths vary between 85 and ~17,570 m (Fig. 4). The shortest dike length was obtained for the dynamic viscosity of 0.3 Pa s, dike width of 0.07 m and $Re = 2.2 \times 10^3$ (Fig. 4, run h). The longest dike length was obtained for a dynamic viscosity of 0.05 Pa s, a dike width of 0.2 m and $Re = 1 \times 10^2$ (Fig. 4, run e). The calculated driving pressures vary from 0.002 to ~0.05 MPa (Fig. 5). The lowest driving pressure was obtained for a dynamic viscosity of 0.05 Pa s and dike width of 0.2 m (Fig. 5, run e). The highest driving pressure was obtained for a dynamic viscosity of 0.3 Pa s and dike width of 0.2 m (Fig. 5, run g). The calculated dike propagation rates vary between 0.0008 and ~0.1 m/s (Fig. 5). The lowest dike propagation velocity for laminar flow condition was obtained for a dynamic viscosity of 0.05 Pa s and dike width of 0.2 m (Fig. 5, run a). The highest dike propagation velocity was obtained for a dynamic viscosity of 0.3 Pa s and dike width of 0.07 m (Fig. 5, run d).

4.2. Turbulent flow model conditions

The turbulent models start by calculating the dike emplacement duration (Eq. (4)) for different dike widths (see Table 1) by using different flow rates. The calculated emplacement durations for the

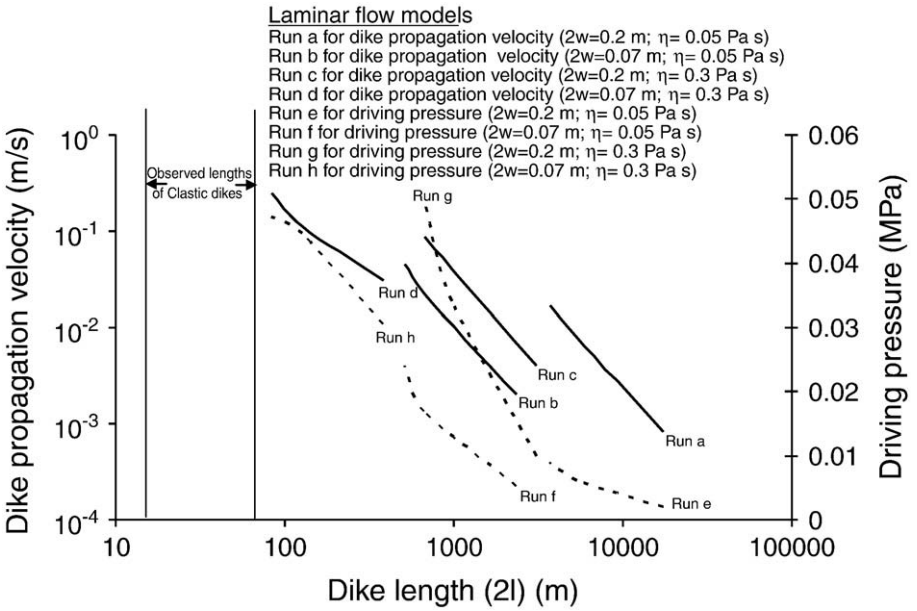

Fig. 5. Results of the laminar propagation model, showing the dike propagation velocity $\left(\frac{dl}{dt} = \frac{2}{3} C_1 A^{1/2} \left[\frac{G}{(1-\upsilon)\eta}\right]^{1/6} t^{-1/3}\right)$, the driving pressure and the dike length (Eqs. (2) and (4)) plotted on log–linear–log graph. The solid and dashed lines mark the dike propagation velocity and driving pressure, respectively. Two vertical lines represent the range of observed dike lengths.

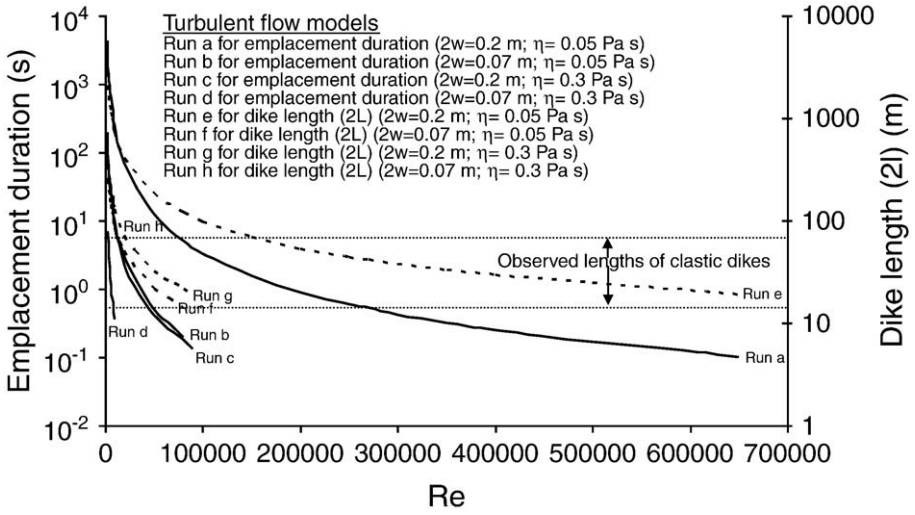

Fig. 6. Results of the turbulent propagation model, showing the emplacement duration and dike length as a function of *Re* number plotted on log–log–linear graph (Eqs. (1), (5) and (6)). The solid and dashed lines mark the emplacement duration and the dike length, respectively. The range of observed lengths of the clastic dikes in the Ami'az Plain study area is marked by two horizontal dashed lines. A lower limit to the driving pressures is marked by a dashed line parallel to the x-axis.

turbulent flow conditions vary between 0.1 and ~4.4×10^3 s, and the corresponding values of *Re* vary between 2.2×10^3 and 650×10^3 (Fig. 6). The upper *Re* was set by using the $2l\approx20$ m limit (see the section "Analytic approaches for dike propagation"). The shortest emplacement duration was obtained for a dike width of 0.2 m, dynamic viscosity of 0.05 Pa s (Fig. 6, run a). The longest emplacement duration was obtained for a dike width of 0.2 m, dynamic viscosity of 0.05 Pa s, and $Re=2.2\times10^3$ (Fig. 6, run a).

The range of emplacement durations calculated by Eq. (4) is used for calculating the ranges of dike length (Eq. (5)), driving pressure (Eq. (6)) and the dike propagation velocity (Fig. 7). The calculated dike lengths range from 20 to ~2820 m (Fig. 6). The longest dike lengths was obtained for a dike width of 0.2 m, dynamic viscosity of 0.05 Pa s, and $Re=2.2\times10^3$ (Fig. 6, run e). The calculated driving pressures vary between 0.2 and ~1.8 MPa (Fig. 7). The highest driving pressure was obtained for a dike width of 0.2 m, dynamic viscosity of 0.3 Pa s, (Fig. 7, run g). The calculated dike propagation velocity varies between 0.2 and ~63 m/s (Fig. 5). The lowest dike propagation rate was obtained for a dike width of 0.2 m, and dynamic viscosity of 0.05 Pa s (Fig. 7, run a). The highest dike propagation velocity was obtained for a dike width of 0.2 m and dynamic viscosity of 0.05 Pa s (Fig. 5, run a).

5. Discussion

5.1. General

The present models of the laminar and turbulent flow conditions provide a tool for estimating the earthquake-induced dike propagation velocity, the dike emplacement duration, and the driving pressures during earthquake events. To get reliable results we used a range of rock and fluid properties that are based on laboratory measurements of viscosity (Levi et al., 2008), published data on soft sediment properties and on our field observations (Table 1).

5.2. Laminar flow conditions

For *Re* between 5×10^2 and 2.2×10^3, almost all dike lengths are above 200 m (Fig. 4). That is the higher limit of the observed dike lengths, excluding run h in which the dike length is less than 200 m.

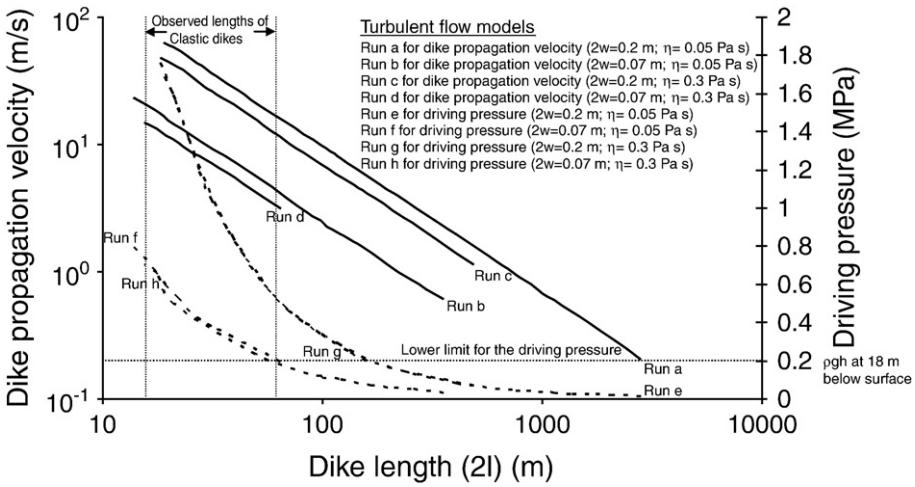

Fig. 7. Results of the turbulent propagation model, showing the dike propagation velocity $\left(\frac{dl}{dt}=\frac{2}{3}C_4\frac{A^{1/6}G^{1/6}t^{-1/3}}{\rho_{fluid}^{1/6}\eta^{1/6}(1-\upsilon)^{1/6}}t^{-1/3}\right)$, the driving pressure and the dike length plotted on log–linear–log graph (Eqs. (5) and (6)). Solid lines mark the dike propagation, and dashed lines mark the driving pressure. Two vertical lines represent the range of observed dike lengths, and the horizontal line shows the limit for the driving pressure.

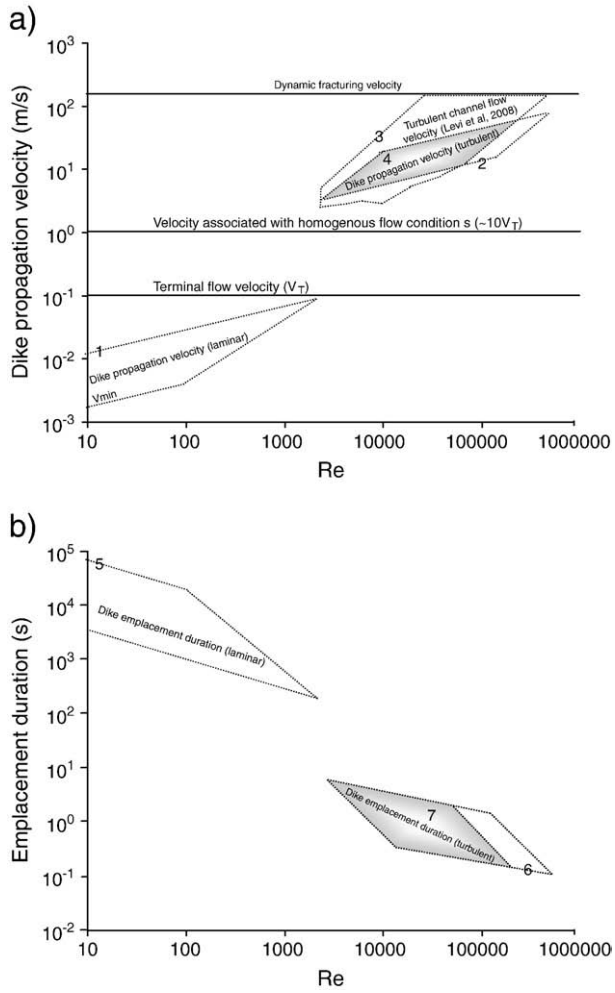

Fig. 8. Possible ranges of propagation velocities and emplacement duration versus the *Re* number, plotted on log–log graph based on the laminar and turbulent propagation models. a) Polygon #1 shows the unlikely ranges of propagation velocities related to the laminar propagation model. Polygon #2 shows the probable ranges of propagation velocities based on the present turbulent propagation model and polygon #3 represents the range of channel flow velocities calculated by Levi et al. (2008). Polygon #4, which is the overlapped area of polygon #2 and polygon #3, represents the most probable range of propagation velocities. b) Polygon #5 shows the unlikely ranges of the emplacement duration related to the laminar propagation model. Polygon #6 shows the probable ranges of the emplacement duration based on the present turbulent propagation model and polygon #7 represents the most probable range of emplacement duration. Numbers along the dash lines represent the larger polygons.

The higher value of the driving pressures (run g; ~0.05 MPa) is about half an order lower than the lower limit of Δp (Fig. 5). Taking into account the physical constraints, Fig. 8a and b demonstrate the higher distribution values of dike propagation velocity (Polygon #1), and the dike emplacement duration (Polygon #5), respectively, calculated by the laminar models (run c).

In Polygon #1 it is shown that for laminar conditions, the higher propagation velocities are between 0.08 and ~0.005 m/s, and the compatible dike emplacement duration between 8 and ~500 s (Polygon #5). Because almost all calculated dike lengths, and the driving pressures are not realistic, it is unlikely that laminar flow conditions could have existed during the clastic-dike propagation in Ami'az Plain.

5.3. Turbulent flow conditions

The turbulent models must satisfy the same physical requirements as the laminar models and obey two constraints: (1) the dike propagation cannot be faster than the dynamic fracturing velocity; and (2) the $Re \sim 2.2 \times 10^3$ sets the lower limit for the flow rate. Most of the calculated lengths of turbulent flow model (runs e, f, and g) are similar to the range of dike lengths measured in the field (Fig. 6). Most of the calculated driving pressures (runs f, g, and h) are above the lower pressure limit (Fig. 7). Hence, turbulent flow is the most appropriate condition for clastic-dike propagation in Ami'az Plain. This is in agreement with the conclusion of Levi et al. (2006a,b) based on independent AMS fabric analyses of the clastic material within the dike. Taking into account the physical constraints mentioned above, the distributions of dike propagation velocity (Polygon #2) and dike emplacement duration (Polygon #6) calculated by the turbulent models are demonstrated in Fig. 8a and in Fig. 8b, respectively. Polygon #2 (Fig. 8a) shows the most probable range of dike propagation velocities, between 3 and ~65 m/s, and the compatible emplacement duration (Fig. 8b), that ranges between 0.2 and ~8.0 s (Polygon #6). Comparing the velocity range (Polygon #3) calculated for a channel flow model (Levi et al., 2008) and the dike propagation velocities (Polygon #2) indicates an overlapping range of velocities (Polygon #4) between 3 and 40 m/s. Converting the range of velocities (Polygon #4) to emplacement duration suggests that the most probable range of dike emplacement duration is 0.5–8.0 s (Polygon #7).

Fig. 9 demonstrates the distribution of driving pressures (Polygon #1) calculated by Eq. (6) with the physical limitations and the distribution of driving pressures (Polygon #2) of the flow channel model (Levi et al., 2008). Likewise, the distribution of the driving pressures (Polygon #3) was constrained by using the elastic crack theory (Levi et al., 2008). A range of Δp (Polygon #4) between 0.8 and 1.8 MPa stands out when the results of the three analytic models are integrated. Consequently, by converting the range of the driving pressure values of 0.8–1.8 MPa, the propagation velocities are between ~4 and ~65 m/s, and the dike emplacement durations are between ~0.8 and 2.0 s. These values are suggested to be the most reliable range of values for clastic dike propagation in Ami'az Plain.

5.4. Lower and upper limits of dike velocities

5.4.1. Low flow velocity range

Propagation velocities of clastic dikes and injection structures (Nichols et al., 1994; Jolly and Lonergan, 2002) may be compared to fluidization velocities. The lower propagation velocities as calculated by the present models are discussed in the context of the minimum velocity of fluidization V_{min} (Wallis, 1969), and terminal velocity of the grains V_T (Richardson, 1971). To estimate the minimum velocity of fluidization and terminal velocity we assumed that all grains are spherical and that during the fluidization process they lose their cohesions forces.

The minimum velocity of fluidization, V_{min}, within the source layer can be estimated by:

$$V_{min} = \frac{0.00059 d^2 \left(\rho_s - \rho_f\right) g}{\eta}, \tag{10}$$

where d is the grain diameter, ρ_s is the density of the grains, ρ_f is the fluid density, and g is the gravitational acceleration constant. Substituting the variables in Table 1 into Eq. (10) resulted in $V_{min} = 3 \times 10^{-7}$ m/s.

The fluidization within the source layer may initiate flow with terminal velocity, V_T and can be estimated by (Wallis, 1969):

$$V_T = \sqrt{\frac{4}{3}\frac{d}{C_F}\frac{\rho_s - \rho_w}{\rho_w}}, \tag{11}$$

where $C_F = 0.44$ for $Re > 1000$, and ρ_w is the water density. Substituting the variables in Table 1 into Eq. (11) resulted in

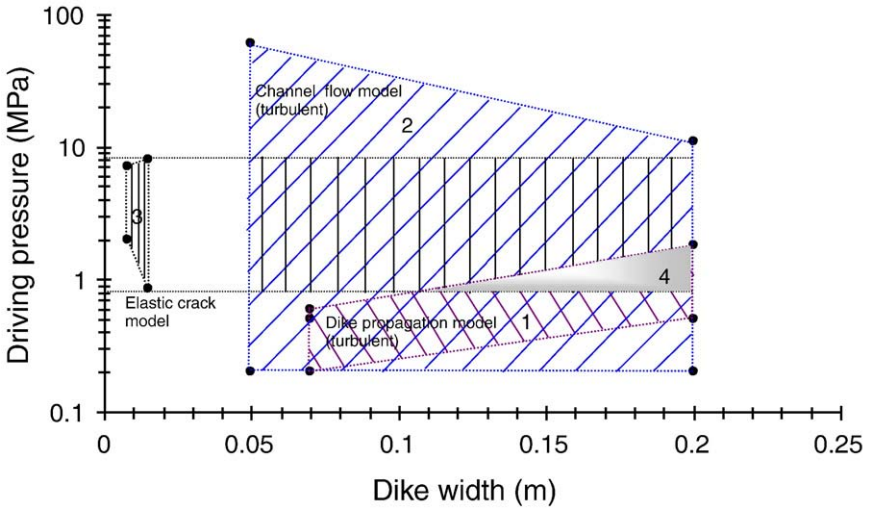

Fig. 9. Possible ranges of driving pressures in the source layer versus the width of the clastic dikes. Polygons #1, #2 and #3 represent calculated driving pressures by using the propagation model of turbulent flow (this study), the channel flow model (Levi et al., 2008), and the elastic crack model (Levi et al., 2008), respectively. Polygon #4, the overlapped area of the three models, represents the most probable range of driving pressures for wide dikes (0.1–0.2 m).

$V_T = 0.1$ m/s. Using the terminal velocity in Fig. 7 resulted in a driving pressure of ~0.1×10^5 MPa and dike length ~8 km.

Because the calculated fluidization velocities are much lower than the velocities needed for satisfying the dike propagation, the latter cannot be estimated by the fluidization velocities alone.

The flow condition is homogeneous only if the average velocity (V_{av}) or the water velocity (V_w) is much greater than the terminal velocity (V_T) ($V_{av} \approx V_w \gg V_T$) (Gallo and Woods, 2004). Hence, in the present models, the flow is likely to be homogeneous when $V_{av} > 10V_T$, e.g., for ~1 m/s (Fig. 9). The lower velocity in Polygon #4 (Fig. 8) starts at ~4 m/s, suggesting that the velocities in the range 4–65 m/s are appropriate for homogenous flow conditions.

5.4.2. High flow velocity range

The present models suggest that the clastic-dike propagation velocity is between ~4–65 m/s and the dynamic fracturing velocity is an upper physical limit (see the section "Analytic approaches for dike propagation"). Substituting the variables in Table 1 into $V_{dynamic} \leq 0.5 (G/\rho_r)^{0.5}$ (e.g., Freund, 1998) resulted in a dynamic fracturing velocity around 130 m/s. The velocity in a 0.2 m wide dike (run a in Fig. 7) may reach half of the dynamic fracturing velocity. Hence, the wider the dike is, its propagation velocity would be closer to the dynamic fracturing velocity. This is in good agreement with Levi et al. (2008) who suggested that clastic dikes could have reached the dynamic fracturing velocity. In their models, the dynamic fracturing velocity was not a physical limitation, because if the dike reached the surface, the velocity of the injected fluid could be even higher than the dynamic fracturing velocity.

5.5. Implications for dike emplacement during earthquake events

5.5.1. The velocities and pressure magnitudes during the hydro-fracturing stage

Earthquake-induced clastic dikes may yield estimates of fluidized particle velocities, and the pressure magnitudes that are associated with an earthquake event. Little is known about these variables, because direct field observations are scarce. More than that, the response of materials to a sudden applied stress is still not well understood (e.g., Sawicki and Mierczyn´ski, 2006), especially for clay-rich sediments (Yılmaz et al., 2004). Yet it is likely that the fluidization in Ami'az Plain resulted from dynamic stresses because static pressure alone could not provide the trigger for fluidization of the Lisan clay-rich sediments, especially because the water content involved in the fluidization could be relatively low (Levi et al., 2006b, 2008).

Transport of particle due to an earthquake event is associated with two consecutive stages: (1) pressure buildup (a nucleation stage), in which the pressure within the source layer builds up until the particles lose their static stability and can start to move as a "fluid"; and (2) propagation stage, in which the pressurized fluid is injected into the host rock forming hydro-fractures. Two different approaches describe the magnitudes of the associated velocities and pressures, the "engineering" and the "geologic" approaches. (1) The engineering approach, based on the soil failure theories (e.g., Seed, 1979), is generally used for estimating the velocities and the pressure magnitudes during the pressure build up stage. In this approach the particle velocities and the pressures within the source layer are estimated by the onset of the pore-pressure buildup, and the shear-strain amplitude required under dynamic loading. (2) The geologic approach estimates the particle velocities and pressures associated with flow and brittle failure processes that occurred during the emplacement stage. In this approach the particle velocities and the pressure magnitudes need to satisfy the condition of hydro-fracture formation.

Approach (1) provides a lower velocity limit required for the nucleation stage within the source layer, and therefore is more conservative than approach (2). Approach (2) deals with the flow of fluidized material and not with the nucleation stage and, hence, with relatively higher magnitudes of velocities and pressures. To illustrate the difference, using fluidized particle velocity of ~0.5 m/s (Cowan, 1999), which represent velocities of approach (1), will result in dike length of about >2 km (Fig. 7).

One injection dike may comprise a few segments arranged co-linearly or in en-echelon architecture. This implies that the parent ("real") dike length is the sum of the dike segment lengths. Careful inspection should be made not to replace two en-echelon segments belonging to one parent dike with two clastic dikes, and vice versa. The average of the dike lengths is about 55 m, and only a few are between 130 and 190 m (Fig. 2). Hence dike length of more than 2 km, calculated by lower propagation velocity (0.5 m/s), is too long for the case of the clastic dikes in Ami'az Plain.

To satisfy the conditions of particle instability within the source layer (approach 1), the effective pore pressure should be equal to or a little above the overburden pressure (Jolly and Lonergan, 2002, and references therein). The overburden pressure above the source layer in Ami'az Plain is ~0.2 MPa. This value, located on the lower limit in Fig. 9 (polygon #1 and polygon #2), may be appropriate for approach

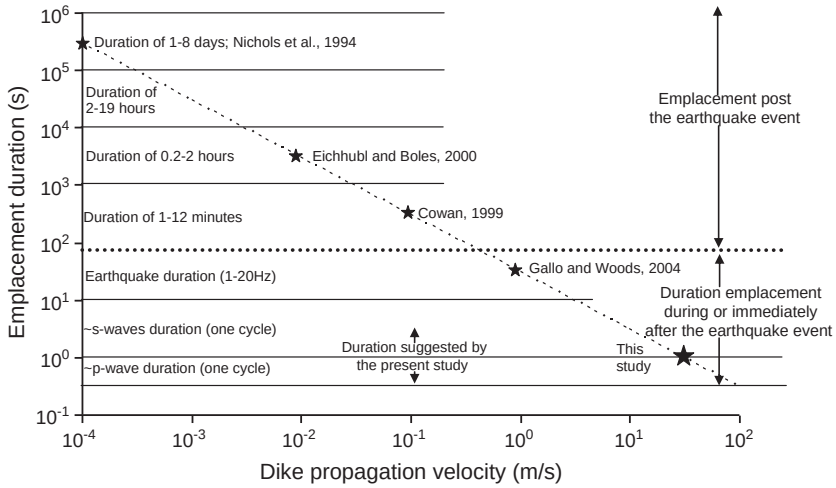

Fig. 10. Dike emplacement duration versus dike propagation velocity on a log–log graph. The emplacement duration of a 30 m long dike, is marked by a filled star. Reported velocities of other injected structures (Nichols et al., 1994; Cowan, 1999; Eichhubl and Boles, 2000; Gallo and Woods, 2004) are also marked. Note that the clastic dikes in Ami'az Plain could have form during the time cycle of the passing acoustic waves through the source layer (see text for details).

(1). Converting the pressure of ~0.2 MPa to dike length resulted in unrealistic length of at least 500 m (Fig. 7). This means that during an earthquake event the magnitudes of the particle velocities and the pressures are at least one order higher than the magnitudes estimated by approach 1.

5.5.2. Emplacement duration of the clastic dikes

The propagation velocities of the clastic dikes help to estimate the emplacement duration of the clastic dikes, and provide insights regarding the processes that generate earthquake-induced clastic dikes. There are only a few studies that estimate the propagation velocity of the fluidized material. Eichhubl and Boles (2000), based on heat transport considerations, estimated an order of 10^{-2} m/s for the paleo-coseismic fluid expulsion velocities. Gallo and Woods (2004) estimated a maximum velocity of ~4 m/s for a dilute sand–water mixture flowing in a vertical conduit. Cowan (1999) suggested that fluidization structures may be associated with velocities in the order of 0.1–1 m/s. Nichols et al. (1994), based on laboratory experiments, showed that fluidization structures may result from unstable fluidization conditions, and that the flow velocity can reach ~5×10^{-4} m/s. Levi et al. (2008) found that the injection velocities, for the last stage of the clastic-dike emplacement, vary between 10 and 130 m/s, and the present study suggests that dike propagation velocities can reach ~65 m/s. Using the above mentioned range of dike propagation velocities, 5×10^{-4} to 100 m/s, and dike length of 55 m (Fig. 3) resulted in 0.6 to 1×10^{5} s for the emplacement duration of the clastic dikes (Fig. 10). This range of emplacement duration may be compared to the duration of an earthquake event with a magnitude larger than 6, which is of the order of several to tens of seconds, close to the epicenter (e.g., Huang and Chen, 2000). Fig. 10 shows that when the emplacement duration of the clastic dikes varies between 1×10^{4} and 1×10^{6} s, they would be emplaced hours to several days after the earthquake event. On the other hand, when the emplacement duration is between 1×10^{-1} and 1×10^{1} s, the dikes would be emplaced between 0.1 and 5 s. This duration range is compatible with the duration of one cycle of the acoustic wave, such as the P and S waves, which is of the order of tenths to several seconds (e.g., Vidale et al., 1995; Horikawa, 2006; McGuire et al., 2008). Based on the arguments mentioned above, the emplacement duration of the clastic dikes is of the order of the cycle duration of the acoustic wave. This mean that the clastic dikes could form not only immediately after the passing waves, but also during the passing waves within the sediments. Levi et al. (2009) suggested that the fluidization process within the source layer is directly related to the impact of the acoustic waves. Clastic dikes such as those in Ami'az Plain which generated directly by the passing waves may be termed "earthquake-induced impact structures".

6. Conclusions

1) The turbulent propagation models for clastic-dike propagation in Ami'az Plain satisfy the physical constraints imposed by field observations, while the laminar propagation models fail to satisfy these constraints, and hence are rejected.
2) The ~0.8 and 2 s duration of the clastic dikes emplacement is similar to that of the acoustic wave cycle that pass through the sediments during an earthquake. This implies that the fluidization and, successively, the formation of clastic dike could form directly by the passing of acoustic waves through the source layer.
3) The propagation models suggest that the propagation velocity of the clastic dike in Ami'az Plain is between ~4 and 65 m/s. The upper velocities are about half of the dynamic fracture velocity, suggesting that wider dikes could attain the dynamic fracturing velocity.
4) An overlapping range of three clastic-dike models suggests that a pressure of 1–2 MPa was generated close to the surface during earthquake events, and is responsible for the fluidization of wet clastic material.
5) Lower velocities and driving pressures of the order of 0.1 m/s and 0.1 MPa, respectively, may be appropriate only for the nucleation stage of fluidization within the source layer. However, such values are not sufficient for the following hydro-fracturing and propagation stage, and therefore a greater pressure is needed for dike injection.

Acknowledgment

This study was supported by the Israeli Ministry of National Infrastructures. We are indebted to the Editor, Mian Liu, Andrew Hurst and anonymous reviewer, for their thorough and very helpful reviews. Discussions with Vladimir Lyakhovsky and Shmuel Marco are highly acknowledged.

References

Anderson, T.L., 1995. Fracture Mechanics, 2nd.edition. CRC Press, Boca Raton, Florida, p. 688.
Arkin, Y., Michaeli, L., 1986. The significance of shear strength in the deformation of laminated sediments in the Dead Sea area. Israel Journal of Earth Sciences 35, 61–72.
Arkin, Y., Michaeli, L., 1986. The significance of shear strength in the deformation of laminated sediments in the Dead Sea area. Israel Journal of Earth Sciences 35, 61–72.
Bahat, D., 1991. Tectono-fractography. Springer-Verlag, Berlin. 354pp.

Bala, A., Raileanu, V., Zihan, I., Ciugudean, Viorica, Grecu, B., 2006. Physical and dynamic properties of the shallow sedimentary rocks in the Bucharest metropolitan area. Romanian Reports in Physics 58 (2), 221–250.

Barenblatt, G.I., 1962. The mathematical theory of equilibrium cracks in brittle fracture. Advances in Applied Mechanics 7, 55–129.

Begin, Z.B., Nathan, Y., Ehrlich, A., 1980. Stratigraphy and facies distribution in the Lisan formation — new evidence from the area south of the Dead Sea. Israel Journal of Earth Sciences 29, 182–189.

Begin, Z.B., Louie, J.N., Marco, S., Ben-Avraham, Z., 2005. Prehistoric seismic basin effects in the Dead Sea pull-apart. The Ministry of National Infrastructures Geological Survey of Israel Report GSI/04/05. 31 pp.

Bell, F.G., 2000. Engineering properties of soils and rocks, 4th edition. Blackwell Science Publishers. 482 pp.

Ben-Menahem, A., Nur, A., Vered, M., 1976. Tectonics, seismicity and structure of the Afro-Eurasian junction — the breaking of an incoherent plate. Physics of the Earth and Planetary Interiors 12, 1–50.

Chetrit, M., 2004. Subsurface structure at the NW coast of the Dead Sea — a geophysical study. M.Sc. thesis, Ben-Gurion University of the Negev, (in Hebrew, English abstract) 66 p.

Cowan, D., 1999. Do faults preserve a record of seismic slip? — A field geologist's opinion. Journal of Structural Geology 21, 2703–2719.

Donald, J.O., 1995. Inner region of smooth pipes and open channels. Journal of Hydraulic Engineering 121, 555–560.

Eichhubl, P., Boles, J.R., 2000. Rates of fluid flow in fault systems-evidence for episodic fluid flow in the Miocene Monterey formation, Coastal California. American Journal of Science 300, 571–600.

Enzel, Y., Kadan, G., Eyal, Y., 2000. Holocene earthquakes inferred from a fan-delta sequence in the Dead Sea graben. Quaternary Research 53, 34–48.

Eyal, Y., Gross, M.R., Engelder, T., Becker, A., 2001. Joint development during fluctuation of the regional stress field in southern Israel. Journal of Structural Geology 23, 279–296.

Freund, L.B., 1998. Dynamic fracture mechanics. Cambridge University Press, Cambridge. 581 p.

Freund, R., Zak, I., Garfunkel, Z., 1968. Age and rate of sinistral movement along the Dead Sea Rift. Nature 220, 253–255.

Gallo, F., Woods, A.W., 2004. On steady homogeneous sand–water flows in a vertical conduit. Sedimentology 51, 195–210.

Gannon, J.A., Masterton, G.G.T., Wallace, W.A., Wood, D.M., 1999. Piled foundations in weak rock. Reprinted in 2004 (London), Sharing Knowledge Building Best Practice, CIRIA Report. 37 p.

Garfunkel, Z., 1981. Internal structure of the Dead Sea leaky transform in relation to plate kinematics. Tectonophysics 80, 81–108.

Gee-Clough, D., Wang, J., Kanok-Nukulchai, 1994. Deformation and failure in wet clay soil: part 3, finite element analysis of cutting of wet clay by Tines. Journal of Agricultural Engineering Research 58, 121–131.

Haase-Schramm, A., Goldstein, S.L., Stein, M., 2004. U–Th dating of Lake Lisan aragonite (late Pleistocene Dead Sea) and implications for glacial East Mediterranean climate change. Geochimica et Cosmochimica Acta 68, 985–1005.

Hofstetter, A., 2003. Seismic observations of the 22/11/1995 Gulf of Aqaba earthquake sequence. Tectonophysics 369, 21–36.

Horikawa, H., 2006. Rupture process of the 2005West Off Fukuoka Prefecture, Japan, earthquake. Earth Planets Space 58, 87–92.

Huang, C.T., Chen, S.S., 2000. Near-field characteristics and engineering implications of the 1999 Chi-Chi earthquake. Earthquake Engineering and Engineering Seismology 2, 23–41.

Hurst, A., Cartwright, J.A. (Eds.), 2007. Implications for Hydrocarbon Exploration and Production: American Association of Petroleum Geologists Memoir, Tulsa. 274 pp.

Jolly, R.J.H., Lonergan, L., 2002. Mechanisms and controls on formation of sand intrusions. Journal of the Geological Society, London 159, 605–617.

Karig, D.E., 1996. Uniaxial reconsolidation tests on porous sediments: mudstones from site 8971. In: Whitmarsh, R.B., Sawyer, D.S., Klaus, A., Masson, D.G. (Eds.), Proceedings of the Ocean Drilling Program, Scientific Results, 149, pp. 363–373.

Ken-Tor, R., Agnon, A., Enzel, Y., Stein, M., Marco, S., Negendank, J.F.W., 2001. High-resolution geological record of historic earthquakes in the Dead Sea basin. Journal of Geophysical Research 106, 2221–2234.

Levi, T., Weinberger, R., Aïfa, T., Eyal, Y., Marco, S., 2006a. Earthquake- induced clastic dikes detected by anisotropy of magnetic susceptibility. Geology 34, 69–72. doi:10.1130/G-22001.1.

Levi, T., Weinberger, R., Aïfa, T., Eyal, Y., Marco, S., 2006b. Injection mechanism of clay-rich sediments into dikes during earthquakes. Geochemistry, Geophysics, Geosystems 7 (2), Q12009–Q12020. doi:10.1029/2006GC001410.

Levi, T., Weinberger, R., Eyal, Y., Lyakhovsky, V., Heifetz, E., 2008. Velocities and driving pressures of clay-rich sediments injected into clastic dykes during earthquakes. Geophysical Journal International 1–13. doi:10.1111/j.1365-246X.2008.03929.x.

Levi, T., Weinberger, R., Eyal, 2009. Decay of dynamic fracturing based on three-dimensional measurements of clastic-dike geometry. Journal of Structural Geology 31, 831–841.

Lister, J.R., 1990. Buoyancy-driven fluid fracture: the effects of material toughness and of low viscosity precursors. Journal of Fluid Mechanics 210, 263–280.

Marco, S., Agnon, A., 1995. Prehistoric earthquake deformation near Masada, Dead Sea graben. Geology 23, 695–698.

Marco, S., Weinberger, R., Agnon, A., 2002. Radial fractures formed by a salt stock in the Dead Sea Rift, Israel. Terra Nova 14, 288–294.

McGuire, J.J., Simons, F.J., Collins, J.A., 2008. Analysis of seafloor seismograms of the 2003 Tokachi-Oki earthquake. Geophysical Research Letters 35 (L14310), 1–5.

Nichols, R.J., Sparks, R.S.J., Wilson, C.J.N., 1994. Experimental studies of the fluidization of layered sediments and the formation of fluid escape structures. Sedimentology 41, 233–253.

Obermeier, S.F., 1996. Use of liquefaction-induced features for Palaeoseismic analysis — an overview of how seismic liquefaction features can be distinguished from other features and how their regional distribution and properties of source sediment can be used to infer the location and strength of Holocene Paleo-earthquakes. Engineering Geology 44, 1–76.

Obermeier, S.F., 1998. Liquefaction evidence for strong earthquakes of Holocene and latest Pleistocene ages in the states of Indiana and Illinois, USA. Engineering Geology 50, 227–254.

Othman, A.A.A., 2005. Construed geotechnical characteristics of foundation beds by seismic measurements. Journal of Geophysics and Engineering 2, 126–138.

Pollard, D.D., 1987. Elementary fracture mechanics applied to the structural interpretation of dykes. In: Halls, H.C., Fahrig, W.F. (Eds.), Mafic Dyke Swarms: Geological Society of Canada, Special Paper, 34, pp. 5–24.

Pollard, D.D., Segal, P., 1987. Theoretical displacements and stress near fracture rocks: with applications to faults, joints, veins, dikes and solution surfaces. In: Atkinson, B.K. (Ed.), Fracture Mechanics of Rocks. Academic Press, London, pp. 277–349.

Porat, N., Levi, T., Weinberger, R., 2007. Possible resetting of quartz OSL signals during earthquakes — evidence from late Pleistocene injection dikes, Dead Sea basin, Israel. Quaternary Geochronology 2, 272–277.

Prandtl, L., 1942. Führer durch die Strömungslehre. Vieweg und Sohn. 648 pp.

Quennell, A.M., 1959a. Tectonics of the Dead Sea Rift: 20th International Geological Congress, pp. 385–405.

Quennell, A.M., 1959b. Tectonics of the Dead Sea Rift: 20th International Geological Congress, pp. 385–405.

Richardson, J.F., 1971. Incipient fluidization and particulate systems. In: Davidson, J.F., Harrison, D. (Eds.), Fluidization. Academic Press, London, pp. 25–64.

Rodrigues, N., Cobbold, P.R., Løseth, H., 2009. Physical modelling of sand injectites. Tectonophysics 474, 610–632.

Rubin, A.M., 1993. Tensile fracture of rock at high confining pressure: implications for dike propagation. Journal of Geophysical Research 98, 15919–15935.

Rubin, A.M., 1995. Propagation of magma-filled cracks. Annual Review of Earth and Planetary Science 23, 287–336.

Sawicki, A., Mierczyn´ski, J., 2006. Developments in modeling liquefaction of granular soils, caused by cyclic loads. Applied Mechanics Reviews 59, 91–106.

Schneider, J.A., Hoyos Jr., L., Mayne, P.W., Macari, E.J., Rix, G.J., 1999. Field and laboratory measurements of dynamic shear modulus of Piedmont residual soils. Behavioral Characteristics of Residual Soils, GSP 92, ASCE, Reston, VA, pp. 12–25.

Seed, H.B., 1979. Soil Liquefaction and cyclic mobility for level ground during earthquakes. Journal of the Geotechnical Engineering Division, ASCE 97, 1249–1274.

Shapira, A., Avni, R., Nur, A., 1993. A new estimate for the epicenter of the Jericho earthquake of 11 July 1927. Israel Journal of Earth Sciences 42, 93–96.

Turcotte, D.L., Schubert, G., 1982. Geodynamics: application of continuum physics to geological problems. John Wiley, Hoboken, N. J. 450pp.

Turcotte, D.L., Emerman, S.H., Spence, D.A., 1987. Mechanics of dyke injection. In: Halls, H.C., Fahrig, W.F. (Eds.), Mafic Dyke Swarms: Geological Society of Canada, Special Paper, 34, pp. 25–29.

Vallejo1, L.E., Lobo-Guerrero, S., 2002. The elastic modili of soils with dispersed oversize. 15th ASCE Engineering Mechanics Conference June 2–5, 2002. Columbia University, New York, NY.

Vidale, J.E., Goes, S., Richards, P.G., 1995. Near-field deformation seen on distant broadband seismograms. Geophisical Research Letters 22, 1–4.

Vigorito, M., Hurst, A., 2010. Regional sand injectite architecture as a record of pore-pressure evolution and sand redistribution in the shallow crust: insights from the Panoche Giant Injection Complex, California. Journal of the Geological Society 167, 889–904.

Vigorito, M., Hurst, A., Cartwright, J., Scott, A., 2008. Regional-scale subsurface sand remobilization: geometry and architecture. Journal Geological Society of London 165, 609–612.

Wallis, G.B., 1969. One-dimensional two-phase flow, 1st ed. McGraw-Hill, New York. 408 pp.

Weinberger, R., Bahat, D., 2008. Relative fracture velocities based on fundamental characteristics of joint-surface morphology. Terra Nova 20, 68–73.

Weinberger, R., Baer, G., Shamir, G., Agnon, A., 1995. Deformation bands associated with dike propagation in porous sandstone. Makhtesh Ramon, Israel. In: Baer, G., Heimann, A. (Eds.), Physics and Chemistry of Dykes, Balkema, Rotterdam, pp. 95–112.

Weinberger, R., Lyakhovsky, V., Baer, G., Begin, Z.B., 2006. Mechanical modelling and InSAR measurements of Mount Sedom uplift, Dead Sea basin: implications for rock-salt properties and diapir emplacement mechanism. Geophysical Journal International 7, Q05014. doi:10.1029/2005GC001185.

Yılmaz, M.T., Pekcan, O., Bakır, B.S., 2004. Undrained cyclic shear and deformation behavior of silt–clay mixtures of Adapazarı, Turkey. Soil Dynamics and Earthquake Engineering 24, 497–507.

Yuan-qiang, C., Xu, L., 2004. Dynamic properties of composite cemented clay. Journal of Zhejiang University Science 5, 309–316.

Zak, I., 1967. The Geology of Mount Sedom, Ph.D. thesis, Hebrew University, Jerusalem.